Supplement of

Atlantic Multidecadal Variability since 1850 is largely externally forced

Yongyao Liang et al.

Correspondence to: Yongyao Liang (YONGYAO.LIANG.2025@mumail.ie)

This supplementary information is to complement the main text by providing detailed descriptions of all datasets used in the analysis, including the observations (Supplementary Table 1) and climate model simulations (Supplementary Table 2-3). The AMV index results from the remaining five SMILEs are presented (Supplementary Fig 1-5).

Details of datasets

Observations

Supplementary Table 1. SST observational datasets.

Dataset	Time coverage	Resolution	Reference
HadSST4	1850-present	5° × 5°	(Kennedy et al., 2019)
NOAA ERSST	1854-present	2° × 2°	(NOAA Extended Reconstructed Sea Surface Temperature (ERSST), Version 5, 2026)
DCENT	1850-present	5° × 5°	(Chan et al., 2024)

Model simulations

Supplementary Table 2. The Single model initial-condition large ensemble (SMILE) simulations.

Project	Size	Horizontal resolution (Lat×Lon)	Historical coverage	Historical forcing	Reference
MPI-GE	100	1.8°×1.8°	1850-2005	CMIP5	(Maher et al., 2019)
CESM1-LENS	40	1° ×1°	1920-2005	CMIP5	(Kay et al., 2015)
CESM2-LENS2	50	1° ×1°	1850-2014	CMIP6	(Rodgers et al., 2021)

CANARI-LE	40	~60km	1950-2014	CMIP6	(Williams et al., 2018)
MIROC6-LE	50	1.4° ×1.4°	1850-2014	CMIP6	(Shiogama et al., 2023)
CanESM5	35	2.8° ×2.8°	1850-2014	CMIP6	(Swart et al., 2019)
FGOALS-g3 Super LE	110	2° ×2.25°	1850-2014	CMIP6	(Zhao et al., 2023)

Supplementary Table 3. The selected model simulations from CMIP6.

Institution	**Model**
AS-RCEC	TaiESMe1
BCC	BCC-CSM2-MR
BCC	BCC-ESM1
CAMS	CAMS-CSM1-0
CAS	CAE-ESM2-0
CAS	FGOALS-f3-L
CAS	FGOALS-g3
CCCma	CanESM5
CMCC	CMCC-CM2-HR4
CMCC	CMCC-CM2-SR5
CMCC	CMCC-ESM2
CSIRO	ACCESS-ESM1-5
CSIRO-ARCCSS	ACCESS-CM2
E3SM	E3SM-1-0
E3SM	E3SM-1-1
E3SM	E3SM-1-1-ECA
EC-Earth-Consortium	EC-Earth3

EC-Earth-Consortium	EC-Earth3-AerChem
EC-Earth-Consortium	EC-Earth-CC
EC-Earth-Consortium	EC-Earth3-Veg
EC-Earth-Consortium	EC-Earth3-Veg-LR
FIO-QLNM	FIO-ESM-2-0
HAMMOZ-Consortium	MPI-ESM-1-2-HAM
INM	IMN-CM4-8
INM	IMN-CM5-0
IPSL	IPSL-CM5A2-INCA
IPSL	IPSL-CM6A-LR
IPSL	IPSL-CM6A-LR-INCA
KIOST	KIOST-ESM
MIROC	MIROC6
MPI-M	MPI-ESM1-2-HR
MPI-M	MPI-ESM1-2-LR
MRI	MRI-ESM2-0
NASA-GISS	GISS-E2-1-G
NASA-GISS	GISS-E2-1-G-CC
NASA-GISS	GISS-E2-1-H
NASA-GISS	GISS-E2-2-G
NASA-GISS	GISS-E2-2-H
NCAR	CESM2
NCAR	CESM2-FV2
NCAR	CESM2-WACCM
NCAR	CESM2-WACCM-FV2
NCC	NorCPM1

NCC	NorESM1-LM
NCC	NorESM1-MM
NIMS-KMA	KACE-1-0-G
NOAA-GFDL	GFDL-CM4
NOAA-GFDL	GFDL-ESM4
NUIST	NESM3
SNU	SAM0-UNICON
THU	CIESM
UA	MCM-UA-1-0

20

Modelling results

The additional SMILEs broadly reinforced the finding that AMV-like variability is predominantly externally forced, with four SMILEs that exhibit limited multidecadal internal variability (Supplementary Fig. 1-4) showing behaviour consistent with CESM2-LENS2 (Fig. 2a-c). Their ensemble means reproduced the timing of major multidecadal transitions in NASST evident in observations, and individual members evolve in phase with one another as well as with the observed AMV. In all cases, the amplitude of variability is weaker than observed, particularly during that 1900-1920 cooling and subsequent warming in HadSST4. While the former mismatch can be explained by a cooling bias in the SST observation (Sippel et al., 2024) and resolved by the bias-corrected SST reconstruction, DCENT (Chan et al., 2024), the latter one remains an open question.

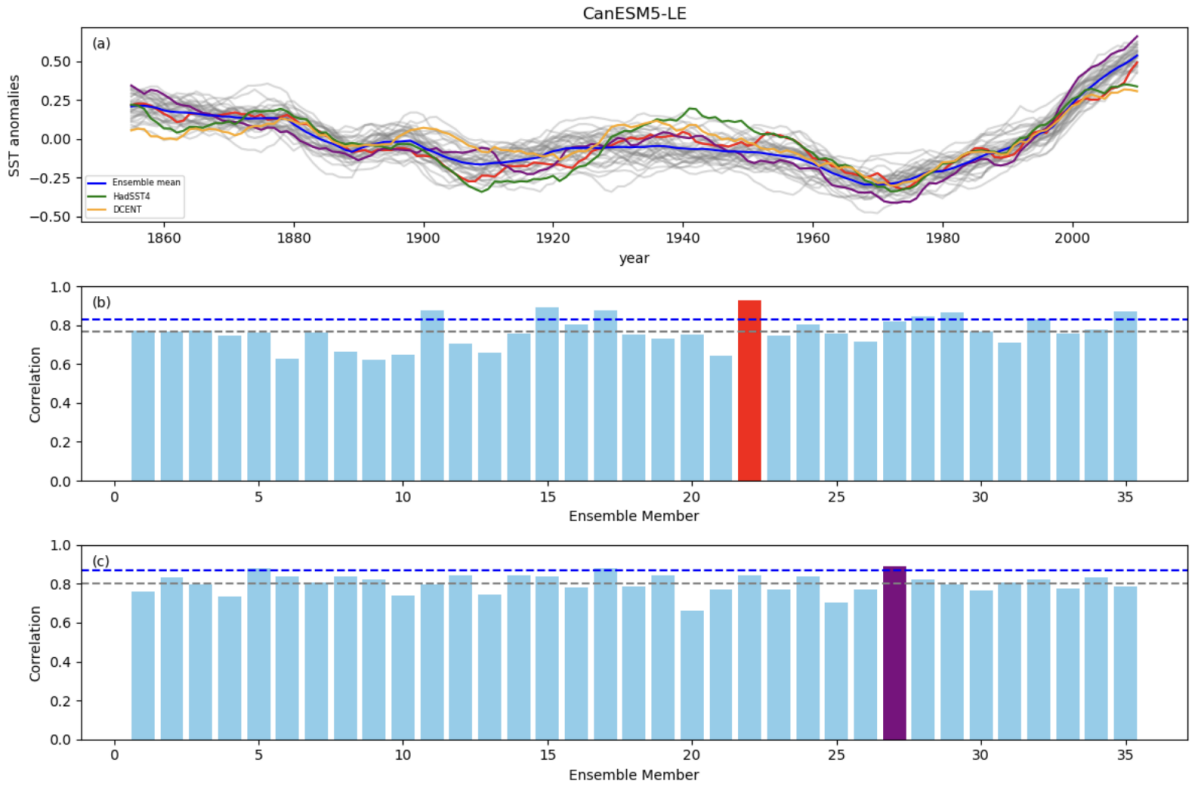

Supplementary Fig. 1. AMV time series and correlation statistics from CanESM5-LE. Same as Fig. 2, but for CanESM5-LE (Swart et al., 2019). **a**, AMV index, calculation is shown in the additional method section. Ensemble mean (blue) represents the externally forced response and is compared with observed AMV from HadSST4 (green) and DCENT (orange). The ensemble member with the highest correlation to HadSST4 (red) and DCENT (purple) is also highlighted. **b**, **c** displace the correlation coefficients between individual members and HadSST4 and DCENT respectively. Blue dashed lines indicate the ensemble mean correlation and grey dashed line indicate the average correlation across members.

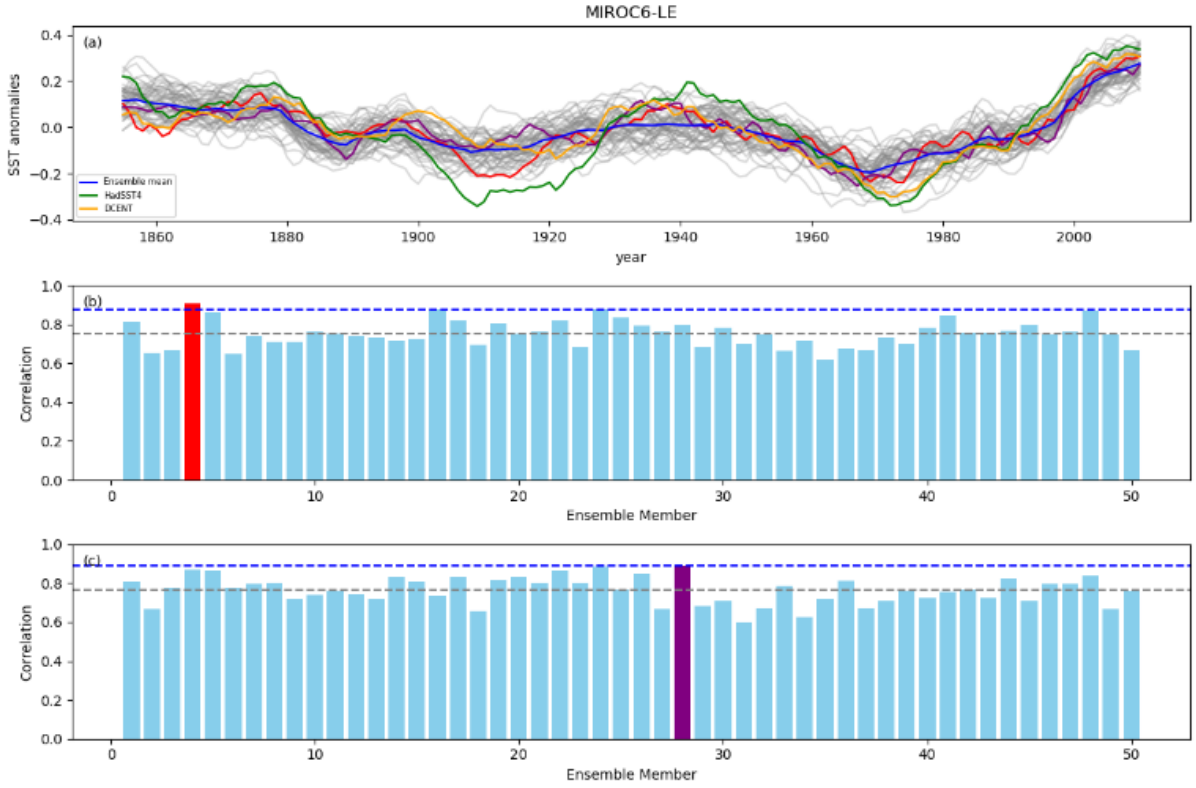

Supplementary Fig. 2. AMV time series and correlation statistics from MIROC-LE. Same as supplementary Fig. 1, but for MIROC6-LE (Shiogama et al., 2023).

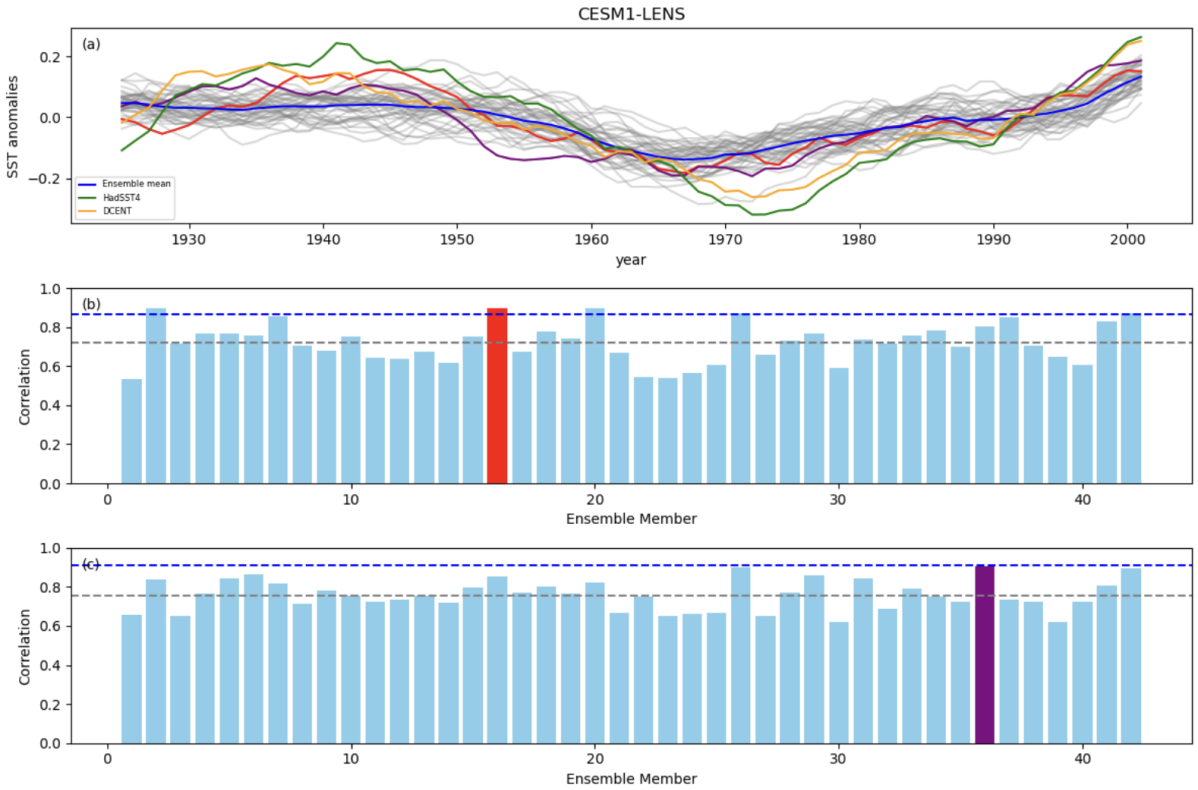

Supplementary Fig. 3. AMV time series and correlation statistics from CESM1-LENS. Same as supplementary Fig. 1 but for CESM1-LENS (Kay et al., 2015). The historical runs of the CESM1-LENS span 1920-2005, accordingly, the linear detrending is performed over this period. After smoothed using a centred 10-year rolling mean, the AMV index covers a period from 1925 to 2001.

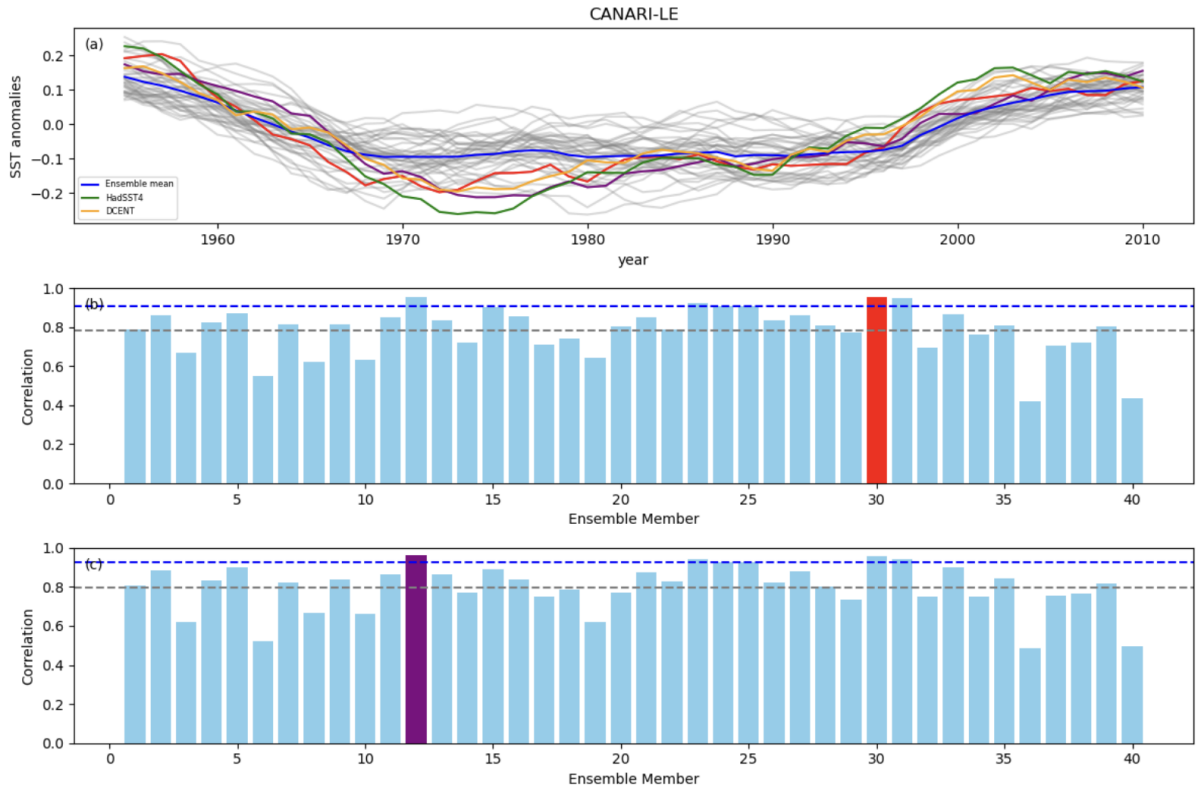

Supplementary Fig. 4. AMV time series and correlation statistics from CANARI-LE. Same as supplementary Fig. 1, but for CANARI-LE (Williams et al., 2018) under the project of Climate change in the Arctic-North Atlantic region and impact in the UK (CANARI), access via UK's data analysis facility JASMIN. The historical runs of the CANARI-LE span 1950-2014, accordingly, the linear detrending is performed over this period. After smoothing by a centred 10-year rolling mean, the AMV indices are available from 1955 to 2010.

In contrast, MPI-GE (Supplementary Fig. 5) supports the interpretation that AMV-like variability may be preliminary caused by internal variability, showing behaviour similar to FGOALS (Fig. 2d-f). Its ensemble members diverge widely and evolve less coherently. The members best correlated with observations show even greater mismatch compared to in FGOALS.

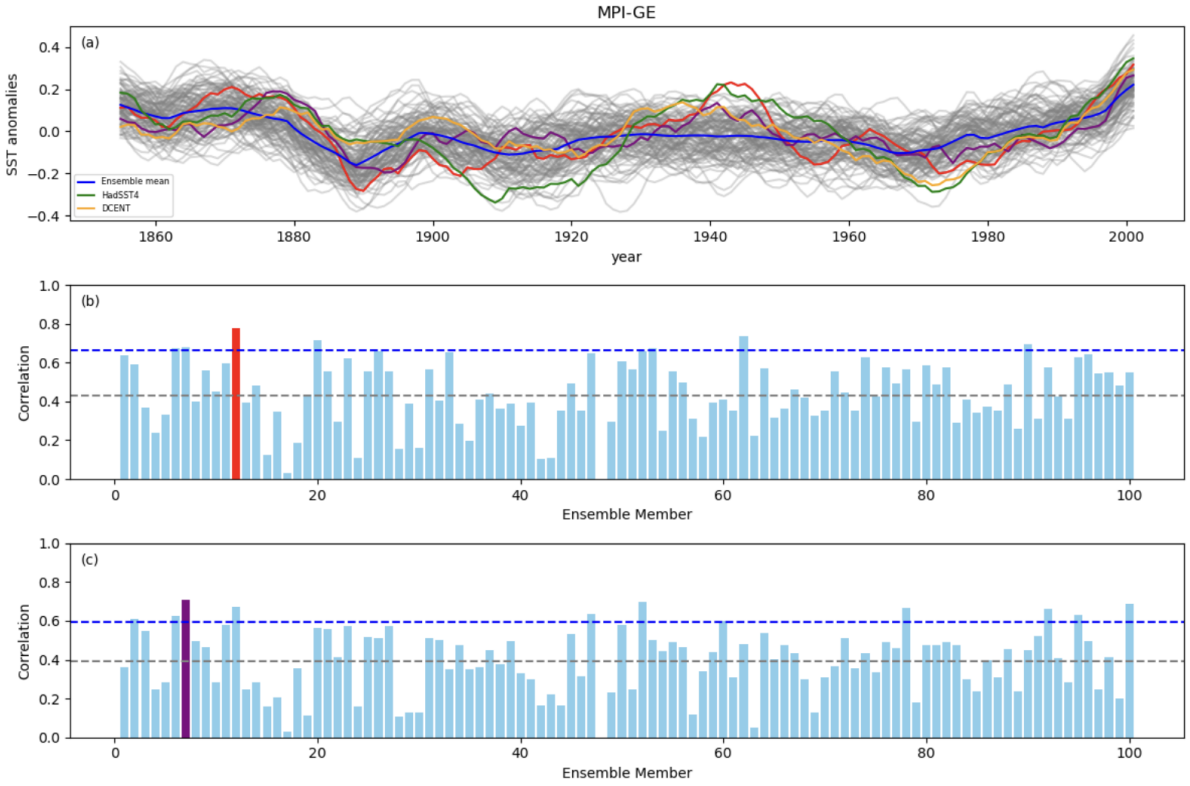

Supplementary Fig. 5. AMV time series and correlation statistics from MPI-GE. Same as supplementary Fig. 1, but for MPI-GE (Maher et al., 2019). The historical runs of the MPI-GE span 1850-2005, accordingly, the linear detrending is performed over this period. After smoothing by a centred 10-year rolling mean, the AMV indices are available from 1955 to 2000.

The divergent behaviour across SMILEs highlights how differences in model physics shape the representation of AMV and affect the balance between internal variability and externally forced responses. While most ensembles reproduce observed AMV and point to an externally forced origin, MPI-GE and FGOALS-LE simulate stronger multidecadal internal variability that obscures the forced signal. Taken together, the results add credence to the hypothesis that AMV is largely externally forced.

Reference

Barghorn, L., Börgel, F., Gröger, M., and Meier, H. E. M.: Atlantic multidecadal variability control on European sea surface temperatures is mainly externally forced, Environ. Res. Lett., 20, 034044, https://doi.org/10.1088/1748-9326/adb6bf, 2025.

Chan, D., Gebbie, G., Huybers, P., and Kent, E. C.: A Dynamically Consistent ENsemble of Temperature at the Earth surface since 1850 from the DCENT dataset, Sci. Data, 11, 953, https://doi.org/10.1038/s41597-024-03742-x, 2024.

Frankcombe, L. M., England, M. H., Kajtar, J. B., Mann, M. E., and Steinman, B. A.: On the Choice of Ensemble Mean for Estimating the Forced Signal in the Presence of Internal Variability, J. Clim., 31, 5681–5693, https://doi.org/10.1175/JCLI-D-17-0662.1, 2018.

NOAA Extended Reconstructed Sea Surface Temperature (ERSST), Version 5: https://www.ncei.noaa.gov/access/metadata/landing-page/bin/iso?id=gov.noaa.ncdc:C00927, last access: 20 January 2026.

Kay, J. E., Deser, C., Phillips, A., Mai, A., Hannay, C., Strand, G., Arblaster, J. M., Bates, S. C., Danabasoglu, G., Edwards, J., Holland, M., Kushner, P., Lamarque, J.-F., Lawrence, D., Lindsay, K., Middleton, A., Munoz, E., Neale, R., Oleson, K., Polvani, L., and Vertenstein, M.: The Community Earth System Model (CESM) Large Ensemble Project: A Community Resource for Studying Climate Change in the Presence of Internal Climate Variability, https://doi.org/10.1175/BAMS-D-13-00255.1, 2015.

Kennedy, J. J., Rayner, N. A., Atkinson, C. P., and Killick, R. E.: An Ensemble Data Set of Sea Surface Temperature Change From 1850: The Met Office Hadley Centre HadSST.4.0.0.0 Data Set, J. Geophys. Res. Atmospheres, 124, 7719–7763, https://doi.org/10.1029/2018JD029867, 2019.

Maher, N., Milinski, S., Suarez-Gutierrez, L., Botzet, M., Dobrynin, M., Kornblueh, L., Kröger, J., Takano, Y., Ghosh, R., Hedemann, C., Li, C., Li, H., Manzini, E., Notz, D., Putrasahan, D., Boysen, L., Claussen, M., Ilyina, T., Olonscheck, D., Raddatz, T., Stevens, B., and Marotzke, J.: The Max Planck Institute Grand Ensemble: Enabling the Exploration of Climate System Variability, J. Adv. Model. Earth Syst., 11, 2050–2069, https://doi.org/10.1029/2019MS001639, 2019.

Peings, Y., Simpkins, G., and Magnusdottir, G.: Multidecadal fluctuations of the North Atlantic Ocean and feedback on the winter climate in CMIP5 control simulations, J. Geophys. Res. Atmospheres, 121, 2571–2592, https://doi.org/10.1002/2015JD024107, 2016.

Robson, J., Sutton, R., Menary, M. B., and Lai, M. W. K.: Contrasting internally and externally generated Atlantic Multidecadal Variability and the role for AMOC in CMIP6 historical simulations, Philos. Trans. R. Soc. Math. Phys. Eng. Sci., 381, 20220194, https://doi.org/10.1098/rsta.2022.0194, 2023.

Rodgers, K. B., Lee, S.-S., Rosenbloom, N., Timmermann, A., Danabasoglu, G., Deser, C., Edwards, J., Kim, J.-E., Simpson, I. R., Stein, K., Stuecker, M. F., Yamaguchi, R., Bódai, T., Chung, E.-S., Huang, L., Kim, W. M., Lamarque, J.-F.,

Lombardozzi, D. L., Wieder, W. R., and Yeager, S. G.: Ubiquity of human-induced changes in climate variability, Earth Syst. Dyn., 12, 1393–1411, https://doi.org/10.5194/esd-12-1393-2021, 2021.

Shiogama, H., Tatebe, H., Hayashi, M., Abe, M., Arai, M., Koyama, H., Imada, Y., Kosaka, Y., Ogura, T., and Watanabe, M.: MIROC6 Large Ensemble (MIROC6-LE): experimental design and initial analyses, Earth Syst. Dyn., 14, 1107–1124, https://doi.org/10.5194/esd-14-1107-2023, 2023.

Si, D. and Hu, A.: Internally Generated and Externally Forced Multidecadal Oceanic Modes and Their Influence on the Summer Rainfall over East Asia, J. Clim., 30, 8299–8316, https://doi.org/10.1175/JCLI-D-17-0065.1, 2017.

Sippel, S., Kent, E. C., Meinshausen, N., Chan, D., Kadow, C., Neukom, R., Fischer, E. M., Humphrey, V., Rohde, R., de Vries, I., and Knutti, R.: Early-twentieth-century cold bias in ocean surface temperature observations, Nature, 635, 618–624, https://doi.org/10.1038/s41586-024-08230-1, 2024.

Swart, N. C., Cole, J. N. S., Kharin, V. V., Lazare, M., Scinocca, J. F., Gillett, N. P., Anstey, J., Arora, V., Christian, J. R., Hanna, S., Jiao, Y., Lee, W. G., Majaess, F., Saenko, O. A., Seiler, C., Seinen, C., Shao, A., Sigmond, M., Solheim, L., von Salzen, K., Yang, D., and Winter, B.: The Canadian Earth System Model version 5 (CanESM5.0.3), Geosci. Model Dev., 12, 4823–4873, https://doi.org/10.5194/gmd-12-4823-2019, 2019.

Williams, K. D., Copsey, D., Blockley, E. W., Bodas-Salcedo, A., Calvert, D., Comer, R., Davis, P., Graham, T., Hewitt, H. T., Hill, R., Hyder, P., Ineson, S., Johns, T. C., Keen, A. B., Lee, R. W., Megann, A., Milton, S. F., Rae, J. G. L., Roberts, M. J., Scaife, A. A., Schiemann, R., Storkey, D., Thorpe, L., Watterson, I. G., Walters, D. N., West, A., Wood, R. A., Woollings, T., and Xavier, P. K.: The Met Office Global Coupled Model 3.0 and 3.1 (GC3.0 and GC3.1) Configurations, J. Adv. Model. Earth Syst., 10, 357–380, https://doi.org/10.1002/2017MS001115, 2018.

Zhao, B., Lin, P., Chen, X. & Wei, J. FGOALS-g3 Super-large ensemble simulation (V3). https://doi.org/10.11922/sciencedb.01332, 2023.